Available online at www.ijournalse.org

Emerging Science Journal

(ISSN: 2610-9182)

Vol. 10, No. 3, June, 2026

Corn Cob-Derived Activated Carbon for Chloramphenicol Removal: An Optimization and Mass Transfer Model Study

Mohamad Razif Mohd Ramli [1, 2, 3*], Abdul Wahab Mohammad [1, 4], Mohd Sobri Takriff [1, 4], Mohd Azmier Ahmad [2], Noor Fazliani Shoparwe [5], Ebenezer I. Oluwasola [6]

[1] *Integrated Water Processing Research Group, Water and Environment Centre, Research Institute of Sciences and Engineering, University of Sharjah, Sharjah 27272, United Arab Emirates.*

[2] *School of Chemical Engineering, Engineering Campus, Tuanku Syed Sirajuddin, Universiti Sains Malaysia, 14300 Nibong Tebal, Pulau Pinang, Malaysia.*

[3] *Faculty of Chemical and Energy Engineering, Universiti Teknologi Malaysia, Skudai 81310, Johor, Malaysia.*

[4] *Chemical and Water Desalination Engineering Program, College of Engineering, University of Sharjah, Sharjah 27272, United Arab Emirates.*

[5] *Gold, Rare Earth and Material Technopreneurship Centre (GREAT), Faculty of Bioengineering and Technology, Universiti Malaysia Kelantan, Jeli Campus, Jeli 17600, Malaysia.*

[6] *Department of Environmental Biotechnology, Faculty of Energy and Environmental Engineering, Silesian University of Technology, Gliwice 44-100, Poland.*

Abstract

This study developed a sustainable activated carbon (AC) from corn cob agricultural waste for efficient chloramphenicol (CP) removal from aqueous solutions and to improve the predictive understanding of the adsorption process. Microwave-assisted physicochemical activation using potassium hydroxide (KOH) was optimized through response surface methodology (RSM), with activation time, microwave radiation power, and impregnation ratio (IR) identified as the key preparation variables. Under the optimal conditions (3.86 min, 616 W, and 2.5 g/g), the resulting AC achieved a yield of 16.6% and a CP adsorption capacity of 20.2 mg/g. The optimized AC exhibited a high BET surface area (832.68 m^2/g), a mesopore-dominated pore structure (mesoporous surface area of 623.45 m^2/g), a pore volume of 0.09067 cm^3/g, and an average pore diameter of 1.93 nm, leading to a maximum experimental adsorption capacity of 20.68 mg/g at 30 °C. In addition, a mass transfer (MT) model was successfully applied to predict an equilibrium adsorption capacity of 21.48 mg/g with a low average error of 3.29% and $R^2 \geq 0.90$. By integrating process optimization with mass transfer modeling, this study improves the understanding of CP adsorption and provides a practical framework for designing efficient, waste-derived adsorbents for antibiotic-contaminated water treatment.

Keywords:
Corn-Cob;
Activated Carbon;
Chloramphenicol;
Adsorption;
Mass Transfer.

Article History:

Received:	27	November	2025
Revised:	11	May	2026
Accepted:	16	May	2026
Published:	01	June	2026

1- Introduction

Chloramphenicol (CP) is a broad-spectrum antimicrobial agent effective against a wide range of bacteria and other microorganisms. CP is produced in large quantities due to its high stability and efficient bacteriostasis for treating human diseases, animals, and shrimp farming [1, 2]. It is particularly unique in the treatment of severe infections such as typhoid fever, meningitis, and other life-threatening illnesses, where other antibiotics are considered ineffective [3]. The increasing demand for CP, particularly in developing nations, owing to its high therapeutic efficiency and cost-

* **CONTACT**: mohamad.razif@utm.my

DOI: https://doi.org/10.28991/ESJ-2026-010-03-08

effectiveness, has resulted in significant chemical pollution of surface water, wastewater, and groundwater [4]. However, due to its genotoxic and carcinogenic effects, such as aplastic anemia, thrombocytopenia, leukopenia, myelosuppression, and baby syndrome, CP has been prohibited in feed production in numerous countries [5]. Hence, the presence of CP in wastewater has become a great concern to environmentalists.

A variety of water treatment processes, such as adsorption, membrane filtration, oxidation processes, and photocatalysis, have been explored in treating antibiotics in wastewater [6, 7]. However, the problems of high cost, large quantity of reagent requirements, frequent electrode replacement, and complex operating procedures have been associated with the membrane filtration, oxidation process, and photocatalysis processes [8-11]. The adsorption process, on the other hand, is a simple process with a broad range of applications and is therefore regarded as an efficient treatment for antibiotics in wastewater with fewer challenges associated with other methods [12].

The adsorption technique is a separation process widely employed in various fields, including purification processes, environmental remediation, and catalysis [13]. The process involves the accumulation of substances at an interface, known as the "adsorbate," while the solid material utilized in the adsorption process is termed the "adsorbent" [14]. The mechanism of adsorption is hinged on the attractive forces between the adsorbate molecules and the surface of the particular adsorbent [15]. The application of activated carbon (AC) as an adsorbent offers a cost-effective and efficient alternative due to its high adsorption capacity, low energy requirements, and minimal byproducts [16, 17]. However, commercial AC, derived from non-renewable resources, is not only expensive but also has limited application. The AC produced from agricultural waste, on the other hand, is a sustainable and cost-effective solution that has garnered significant interest owing to its abundance, cost-effectiveness, and great adsorptive capacities for antibiotic removal, which have been studied extensively [18, 19].

The exceptionally high surface area and porous structure of AC enhance its ability to capture and retain organic pharmaceutical contaminants from wastewater [20, 21]. The porous structure of AC makes it particularly effective at adsorbing the smaller molecules of CP, demonstrating superior adsorption capacities compared to other materials [22]. Despite the growing interest in the adsorption of antibiotics using the AC, there remains a significant research gap in developing general predictive modeling for assessing the concentration of antibiotics at the equilibrium stage and their adsorption capacity, as well as the adsorbent's surface area.

Hence, the need to optimize AC preparation parameters, such as activation temperature, radiation power, activation time, and impregnation ratio, is a critical step for improving adsorption performance using the response surface methodology (RSM) [23]. The RSM is used to identify optimal conditions while minimizing experimental trials [24, 25]. Similarly, mass transfer (MT) is a crucial tool in the study of the adsorption process, particularly for removing pharmaceutical compounds from aqueous solutions using different adsorbents [21, 26]. The process efficiency is significantly influenced by the rate at which pharmaceutical molecules are transferred from the bulk solution to the adsorbent's surface, followed by their diffusion within the material's porous structure. Several factors have been identified to affect this process, which include pore size, surface area, and the physicochemical interactions between the adsorbent and adsorbate.

The present study adopts a theory-driven framework that integrates statistical optimization and MT principles to elucidate the adsorption behavior of CP on microwave-assisted corn cob-derived activated carbon (CCAC). RSM was applied based on the theoretical premise that the physicochemical properties of AC and its adsorption performance are governed by both individual and interactive effects of key preparation variables, namely activation time, microwave radiation power, and KOH impregnation ratio (IR). This approach enables systematic evaluation of nonlinear relationships between preparation conditions and adsorption responses while minimizing experimental runs.

From an adsorption theory perspective in the current research [27], the removal of pharmaceutical compounds is primarily controlled by surface area availability, pore size distribution, and surface functional groups, which collectively influence pore filling, surface diffusion, and adsorbate–adsorbent interactions. Accordingly, a comprehensive characterization of surface area, pore structure, morphology, functional groups, proximate analysis, and elemental composition was conducted to link material properties with adsorption performance. In addition, an MT model was developed to describe the transport of CP molecules from the bulk solution to the CCAC surface and into internal pore structures [28], thereby providing a mechanistic interpretation of adsorption kinetics beyond empirical observations.

2- Material and Methods

2-1- Materials and Chemicals

Corn cob (CC) from the sweet corn species was sourced from Changkat Jering, Perak, Malaysia. Chloramphenicol (CP), potassium hydroxide (KOH), and phosphoric acid (H_3PO_4) were all obtained from Sigma Aldrich. CP served as the adsorbate, while KOH was employed for the chemical activation step and to adjust the pH of the solution, while H_3PO_4 was also used for pH regulation of the solution.

2-2- Experimental Activities

The flowchart of the research methodology that was used to achieve the study's aims is shown in Figure 1.

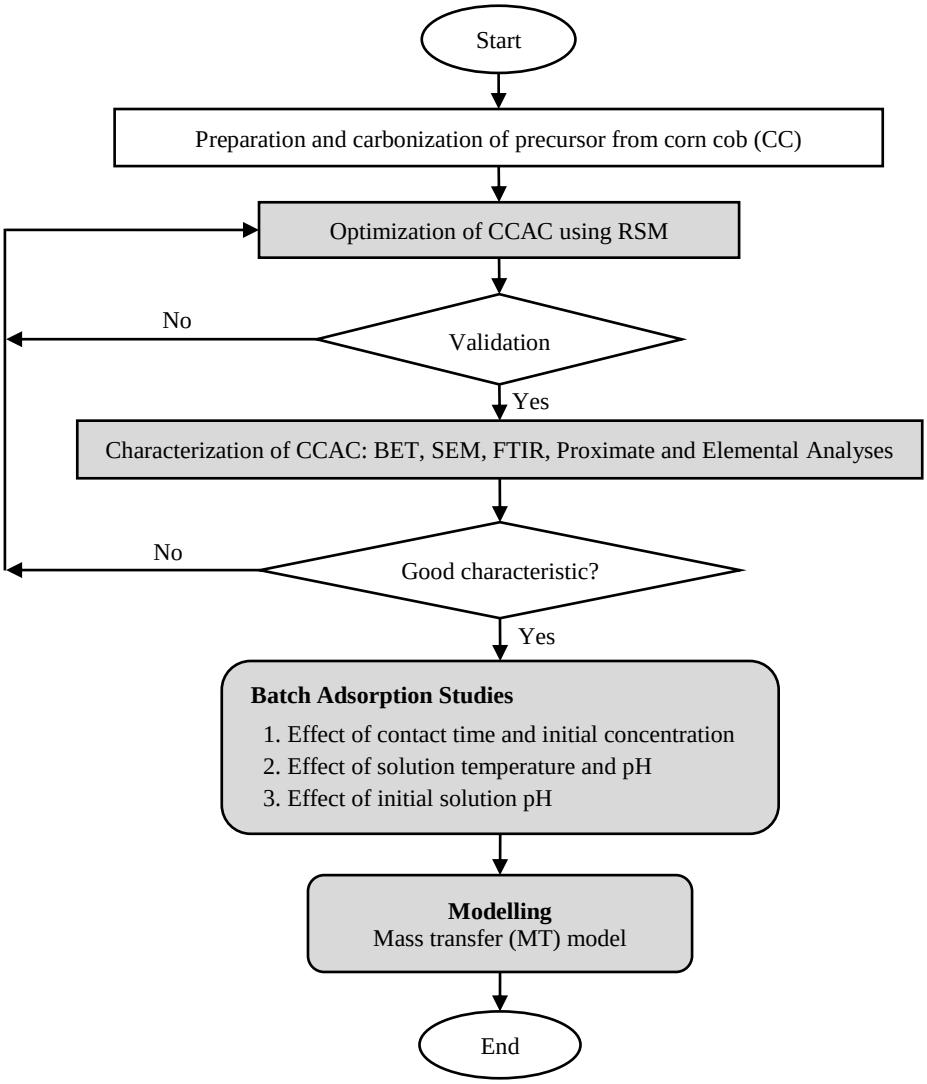

Figure 1. Flowchart of overall experimental work

2-3- Design of Experiment

RSM based on a face-centred central composite design (CCD) was applied to optimize the preparation conditions of CCAC. Design Expert software (Version 13, STAT-EASE Inc., Minneapolis, USA) was utilised to develop an accurate second-order quadratic model with a minimal number of experimental runs. The CCAC was synthesized through a physicochemical approach, considering three factors: activation time (X_1), microwave radiation power (X_2), and KOH impregnation ratio, IR (X_3). The evaluated responses were CP removal (Y_1) and CCAC yield (Y_2). A face-centred CCD with three factors was coded to the (-1, 0, +1) interval, where the low and high levels were coded as -1 and +1, respectively. The variables, experimental range, and level of the variable are summarised in Table 1. The model's performance was assessed based on the responses of CP removal efficiency and CCAC yield.

Table 1. Coded and actual levels of the variables of CCAC

Parameters	Units	Code	Coded level and limits		
			-1	0	1
Activation time	Minute (min)	X_1	2	4	6
Microwave radiation power	Watt (W)	X_2	264	440	616
IR	g/g	X_3	0.5	1.5	2.5
CP removal	mg/g	Y_1	-	-	-
CCAC yield	%	Y_2	-	-	-

The experimental design matrix, along with the corresponding responses generated using the CCD approach are presented in Table 2.

Table 2. Proposed runs matrix and results

Run	X_1: Activation time (min)	X_2: Microwave radiation power (W)	X_3: Impregnation ratio, IR (g/g)	Y_1: CP removal (mg/g)	Y_2: Yield (%)
1	2	264	0.5	3.59	26.11
2	6	264	0.5	8.58	25.23
3	2	616	0.5	15.04	18.19
4	6	616	0.5	14.15	15.57
5	2	264	2.5	4.38	25.44
6	6	264	2.5	12.01	16.37
7	2	616	2.5	17.49	20.15
8	6	616	2.5	18.51	8.69
9	2	440	1.5	7.14	26.41
10	6	440	1.5	6.51	15.34
11	4	264	1.5	5.88	19.17
12	4	616	1.5	20.09	10.65
13	4	440	0.5	5.39	23.99
14	4	440	2.5	12.88	24.14
15	4	440	1.5	8.20	24.84
16	4	440	1.5	7.88	22.12
17	4	440	1.5	7.50	24.61
18	4	440	1.5	5.12	19.64
19	4	440	1.5	7.54	22.14
20	4	440	1.5	5.91	20.11

2-4- Sample Preparation

The dried CC was crushed using a biomass crusher (Model Crusher 50 HP) and sieved to a uniform particle size of 2 cm. Carbonization of the dried CC was carried out in a vertical furnace (Model Carbolite) at 550 °C under a continuous nitrogen (N_2) flow (150 mL/min) to produce char in an inert atmosphere. The obtained char was then chemically activated by impregnation with KOH at varying impregnation ratios (IR), which is defined as the mass ratio of KOH to char. The impregnated samples were soaked for 8 h and subsequently dried at 110 °C for 24 h, followed by microwave-assisted activation (Model EMM2001W, Sweden) under a continuous carbon dioxide (CO_2) flow (150 mL/min), where CO_2 functioned as the physical activating gas. Finally, the corn cob–derived activated carbon (CCAC) was washed with 0.1 M HCl and deionised water until a near neutral pH (6.5–7) was achieved and then oven-dried. The final yield of CCAC was determined as the mass ratio of dried AC (W_F) to the initial biomass (W_i) in grams as expressed in Equation 1:

$$Yield = \frac{W_F}{W_i} \times 100\% \quad (1)$$

2-5- Sample Characterization

Physicochemical properties of samples were evaluated using several analytical techniques. Surface area, pore volume, and pore size distribution were measured using N_2 adsorption-desorption (Micromeritics ASAP, USA) after degassing the samples at 350°C for 6 h under vacuum. Surface morphology and pore structure were observed using scanning electron microscopy (SEM, Quanta 450 FEG, Netherlands). Thermal stability and proximate composition (which comprises volatile matter, moisture, fixed carbon, and ash content) were determined via simultaneous thermal analysis (STA 6000, Perkin Elmer, USA). Elemental composition was analyzed using energy-dispersive X-ray spectroscopy (EDX, Perkin Elmer Series II 2400, USA). The functional groups present on the sample surfaces were characterized using Fourier-transform infrared spectroscopy (FTIR, Shimadzu Prestige 21, Japan) with the KBr pellet technique.

2-6- Effect of Contact Time and Initial Concentrations

A batch adsorption optimization experiment on the CCAC was conducted to evaluate the adsorption capacity of CCAC against CP. In the study, 0.2 g of CCAC was added to a 250 mL conical flask containing 200 mL of varied initial CP concentrations (5, 10, 15, 20, 25, and 30 mg/L). The mixtures in the conical flasks were agitated in a water-bath

shaker at 30 °C and 100 rpm for 7 h. Subsequently, samples were taken at specific time intervals from (0, 0.25, 0.5, 1, 2, 3, 6, and 7 h) and the CP concentrations were measured using a UV–Visible spectrophotometer (Shimadzu UV-1800, Japan). To conduct the equilibrium studies, the adsorption capacity q_e, was determined using Equation 2:

$$q_e = \frac{(C_0 - C_e)V}{W} \quad (2)$$

While the CP removal was calculated by Equation 3:

$$CP\ removal\ (\%) = \frac{(C_e - C_t)}{C_t} \times 100\% \quad (3)$$

where, C_0 is the initial concentration of the adsorbate in the liquid phase (mg/L), C_e is the equilibrium concentration of the adsorbate in the liquid phase (mg/L), C_t is the liquid phase concentration at time, t (mg/L), V is the volume of the solution (mL), and $W$is the mass of CCAC (g).

2-7- Effect of Temperatures and Solution pH

The CP adsorption procedures were conducted at three different temperatures (30, 45, and 60 ºC) by adjusting the temperature controller while maintaining the other operating parameters, such as CCAC dosage, initial concentration, and rotational speed as constant. The effect of pH variation on CP adsorption was conducted at pH of 2, 4, 6, 8, 10, and 12 (using H_3PO_4 and KOH to adjust the pH) at a constant temperature.

2-8- Mass Transfer Modeling

The MT model was developed to describe the removal behavior of CP. By integrating MT principles, the model effectively predicts the adsorbent's surface area and can be expressed by Equation 4:

$$C = C_e - e^{-t(k_{MT} - a_{MT}k_m)(C_e - C_o)} \quad (4)$$

where, C is the calculated concentration (mg/L), k_{MT} denotes the adsorption process rate during pore diffusion (s^{-1}), a_{MT} represents the adsorption surface area (m^2/g), k_m corresponds to the mass transfer coefficient ($mg \cdot m \cdot L^{-1}\ s^{-1}$). The parameters were estimated by fitting the experimental data to Equation 4 using Polymath® software (Version 6.2, CACHE Corp., USA).

3- Results and Discussion

3-1- Regression Model Development

The relationship between CCAC preparation conditions, CP removal (Y_1), and CCAC's yield (Y_2) was investigated using face-centred CCD. Activation time (X_1), radiation power (X_2), and impregnation ratio, IR (X_3) are the conditions under which CCAC was prepared. Based on the sequential model sum of squares, the highest-order polynomial was selected when additional terms were significant, and the model showed no aliasing. The quadratic model was identified as the best fit for all responses. Figures 2-a and 2-b illustrate the diagnostic plots of predicted versus actual values for CP removal and CCAC yield, respectively.

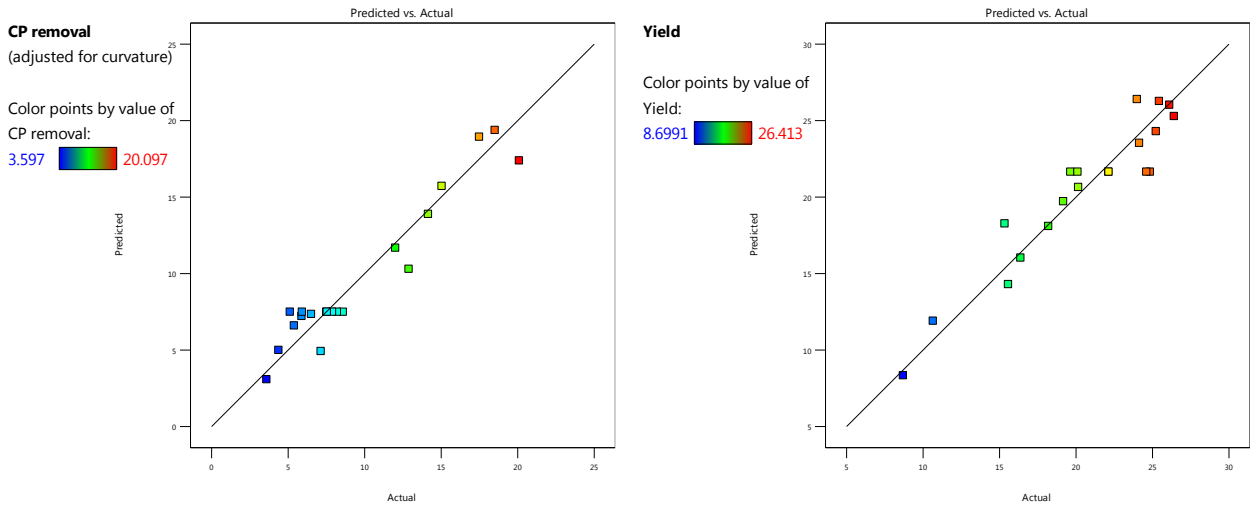

(a) (b)

Figure 2. Regression plots of predicted versus actual for (a) CP removal and (b) CCAC yield

The regression analysis shows agreement between the model responses and the experimental data. Four statistical parameters, which are correlation coefficient (R^2), adjusted correlation coefficient (Adj. R^2), standard deviation (SD), and adequate precision (AP), were employed to validate the models. A higher R^2 value closer to unity indicates better model quality [29], while Adj. R^2 provides an improved measure of R^2 by excluding the influence of insignificant variables. The models exhibited exceptionally high R^2 and Adj. R^2 for both responses with Y_1 (0.9225 and 0.8528, respectively) and Y_2 (0.9038 and 0.8172, respectively). These results suggest that 92.25 % of the variation in CP removal and 90.38 % of the variation in CCAC yield were explained by the experimental variables.

For SD, the more its value approaches zero, the less the predicted values deviate from the actual experimental value [25]. On the other hand, the AP parameter, which measures the signal-to-noise ratio, is incredibly helpful in determining whether the developed model is sufficient for estimating responses or not. A relatively low value of the SD and high AP for CP removal (1.92,11.99), and CCAC yield (2.18, 11.74), were observed, respectively. A similar trend was reported by Abd Khalil et al. [30], who used AC derived from coffee ground waste to adsorb oxytetracycline and achieved strong predictive capability with low SD values using RSM. The high predictive reliability of the developed models is statistically supported by the close agreement between experimental and predicted data, as well as the robust signal strength of the models. The low SD values further indicate high experimental reproducibility, providing a reliable foundation for model development.

3-2- Analysis of Variance (ANOVA)

ANOVA was employed to evaluate the extent of significance and adequacy of the models. The ANOVA results confirmed the suitability of the quadratic model for all responses. A p-value less than 0.05 coupled with a high F-value suggests that the model terms were statistically significant, and the data were not random [31].

All the developed models demonstrated statistically significant results, with p-values below 0.05, as presented in Tables 3 and 4. According to Table 3, the significant terms for this response were X_2, X_3, X_1X_2, and X_2^2. Based on the F-value, this response was highly influenced by X_2 (69.94) and followed by X_3 (9.26). Based on Table 4, the significant terms were X_1, X_2, X_1X_3, X_2^2, and X_3^2. F value revealed that this response was primarily affected by X_2 of 32.23 and X_1 of 26.03. For all the responses studied, the lack of fit was not significant. It is preferable to have an insignificant result for the test of lack of fit, as this indicates the significant effects of variables on the investigated responses and shows that the developed models adequately fit the experimental data.

Table 3. ANOVA results for the response of CP removal by CCAC

Source	Sum of square	Mean square	F Value	Prob >F
Model	440.18	48.91	13.23	0.0002
X_2	258.45	258.45	69.94	< 0.0001
X_3	34.22	34.22	9.26	0.0124
X_1X_2	19.49	19.49	5.27	0.0445
X_2^2	63.52	63.52	17.19	0.0020
Residual	**36.96**	**3.70**		

Table 4. ANOVA results for the response for CCAC's yield

Source	Sum of square	Mean square	F Value	Prob >F
Model	444.64	49.40	10.44	0.0005
X_1	123.18	123.18	26.03	0.0005
X_2	152.54	152.54	32.23	0.0002
X_1X_3	36.20	36.20	7.65	0.0199
X_2^2	93.77	93.77	19.81	0.0012
X_3^2	30.23	30.23	6.39	0.0300
Residual	**47.33**	**4.73**		

3-3- Three-Dimensional (3D) Surface Plot

The ability to analyze the pattern of variables affecting responses in 3D plots is one of the advantages of RSM. Radiation power and IR affected the responses of CP removal by CCAC, whereas for CCAC's yield, activation time, and radiation power were the dominant factors. Figure 3-a demonstrates that radiation power and IR are inversely and directly proportional to CP removal, respectively, while Figure 3-b shows that activation time and radiation power gives impact on CCAC's yield. An increase in CP removal was observed with higher radiation power, which can be attributed

to cracking reactions facilitating the release of heavy volatile compounds from the CCAC matrix. This process facilitates the formation of vacant sites and pores, thereby enhancing the adsorption capacity. However, extreme conditions of radiation power led to the rupture of the CCAC pore's structure. When there are high concentrations of IR on CCAC, the KOH particles move rapidly, eventually leading to collisions. Consequently, the particles acquire kinetic energy, enabling them to accelerate and overcome the blockage in the pores, leading to a substantial increase in the rate of removal. Rashidi & Yusup [32] stated that a higher ionization rate can facilitate the formation of additional pores by allowing an increased influx of K^+ ions into the char, which leads to an increase in the removal efficiency.

From Figure 3-b, the CCAC's yield was found to be the maximum yield at shorter activation time and low radiation power. By increasing activation time, the volatilization process was prolonged, thereby reducing CCAC's yield even further. In contrast, Aziz et al. [33] concluded that prolonged activation time may be attributed to the volatilization of surface carbon atoms, which becomes predominant, leading to increased adsorbent weight loss and the formation and widening of pores. Consequently, this phenomenon enhances the availability of the adsorbent surface area, resulting in higher adsorbate removal. For CP removal, activation time must be optimized to balance the formation of pore structure and the preservation of CCAC's yield. Shorter activation times enhance yield but result in insufficient surface area for effective adsorption, while excessively long activation times may reduce adsorption efficiency due to structural degradation and reduced surface area [34].

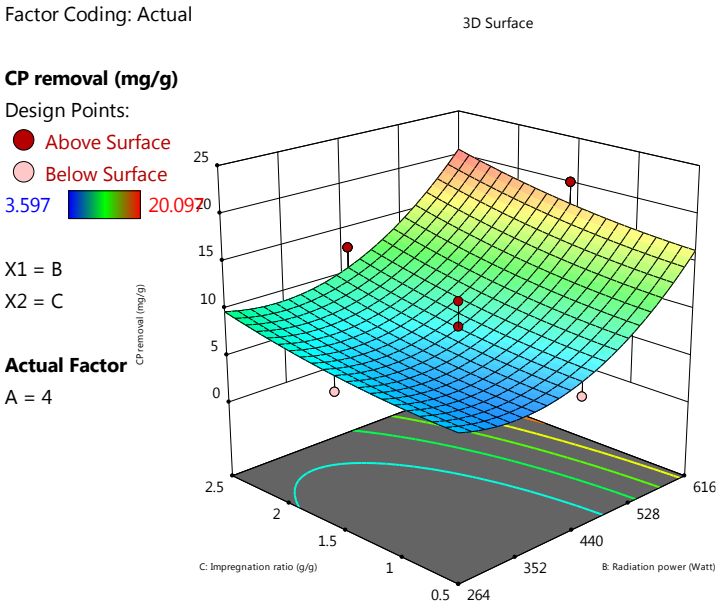

(a)

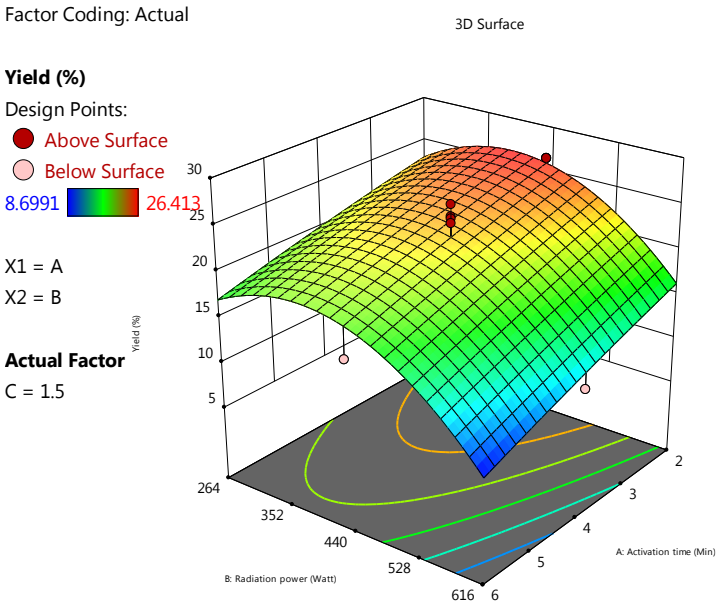

(b)

Figure 3. Three-dimensional response plot for (a) CP removal (effect of radiation power and IR), activation time = 4 min, and (b) CCAC's yield (effect of activation time and radiation power, IR = 1.5)

3-4- Optimum Conditions

The optimal conditions for CCAC preparation were established using RSM to maximize CP removal while maintaining an acceptable CCAC yield. The selected variables, including X_1, X_2 and X_3 were identified as critical factors influencing the activation process, as supported by preliminary experiments and previous literature [35]. The optimal conditions identified were 3.86 minutes for activation time, 616 W for radiation power, and 2.5 g/g for IR, resulting in CP removal of 20.2 mg/g and a CCAC yield of 16.6%, as shown in Table 5. Mohd Zainorin et al. [36] reported a low yield of mangrove wood–derived activated carbon due to extensive thermal cracking, which promoted a higher degree of decomposition over prolonged activation time. Although the optimized condition resulted in a relatively moderate yield, the reduction in yield is associated with enhanced pore development and surface area formation during activation. In practical applications, a balance between yield and adsorption capacity should be considered depending on economic priorities and precursor cost. Given the abundance and low cost of CC biomass, the improved adsorption efficiency may offset the reduced yield for large-scale implementation. The low error percentages across all responses confirm that the developed models accurately predicted the experimental outcomes.

Table 5. Optimum conditions for optimized CCAC

Variables			Responses					
			CP removal Y_1 (mg g^{-1})			CCAC yield Y_2 (%)		
Activation time, X_1 (min)	Microwave radiation power, X_2 (W)	IR, X_3 (g/g)	Predicted	Actual	Error (%)	Predicted	Actual	Error (%)
3.86	616	2.5	20.50	22.30	1.49	14.8	16.6	10.84

3-5- Characterizations

The samples were characterized by their surface morphology, chemical composition, and surface properties to assess their adsorption performance. BET analysis revealed that raw CC had a very low surface area of 2.37 m^2/g and total pore volume of 0.0031 cm^3/g, indicating a dense and nonporous structure. Carbonization of CC to produce char increased the BET surface area to 82.49 m^2/g and mesoporous area to 46.48 m^2/g, with a total pore volume of 0.0425 cm^3/g and average pore diameter of 1.85 nm. Subsequent microwave-assisted chemical activation of char with KOH and CO_2 produced CCAC with significantly enhanced textural properties, achieving a BET surface area of 832.684 m^2/g, with an external (mesopore-associated) surface area of 623.45 m^2/g, indicating hierarchical pore development despite the predominantly microporous structure (average pore diameter = 1.93 nm). The physicochemical activation of char in microwave induced the following chemical reactions [37]:

$$2KOH\ (aq) \rightarrow K_2O\ (s) + H_2O\ (l) \quad (5)$$

$$H_2O\ (l) + C\ (s) \rightarrow CO\ (g) + H_2\ (g) \quad (6)$$

$$CO_2\ (g) + K_2O\ (s) \rightarrow K_2CO_3\ (s) \quad (7)$$

$$K_2CO_3\ (s) \rightarrow K_2O\ (s) + CO_2\ (g) \quad (8)$$

$$CO_2\ (g) + C\ (s) \rightarrow 2CO\ (g) \quad (9)$$

$$K_2O\ (s) + 2C\ (s) \rightarrow K\ (s) + 2CO\ (g) \quad (10)$$

$$K_2CO_3\ (s) + C\ (s) \rightarrow 2K\ (s) + 3CO\ (g) \quad (11)$$

The synergistic effect of KOH and CO_2 during activation facilitated pore formation through reactions generating CO, CO_2 , and metallic potassium, which bombarded and widened the pore network [38]. The substantial increase in surface area provided numerous active sites for CP adsorption, with the pore size well-suited to the dimensions of CP molecules (1.0–1.2 nm length, 0.5–0.7 nm width). Ramli et al. [37] also reported the effect of CO_2 in enhancing porosity through gasification, where carbon reacts with CO_2 to produce CO, leading to a substantial increase in surface area. SEM images (Figures 4-a and 4-c)) illustrate the morphological surface of the samples. Raw CC exhibited a dense, uneven surface with no apparent pores. After carbonization, char displayed initial pore formation, while CCAC showed a well-developed porous network with enlarged pore structures resulting from the combined microwave radiation and chemical activation process [39]. According to Nasehir Khan et al. [40], the development of these pores is attributed to the evaporation of moisture and volatile components during the carbonization and activation stages.

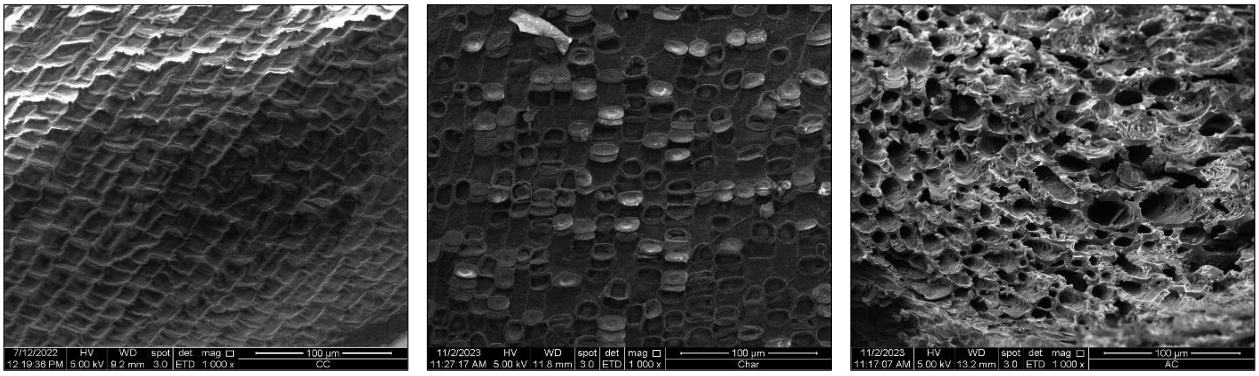

(a) (b) (c)

Figure 4. SEM micrographs of (a) CC, (b) Char, and (c) CCAC at a magnification of 1000x

Table 6 presents the results of proximate and elemental analysis of the CC, char, and CCAC. Proximate analysis revealed that CC consists of 6.468 % moisture, 72.234 % volatile matter, 18.212% fixed carbon, and 3.09 % ash. An increased fixed carbon content results in an augmented formation of AC's skeletal structure, thereby contributing to an elevated surface area [41]. Initially, the CC has the highest volatile matter but with low fixed carbon content, but as the CC was carbonized up to 550 °C in a vertical furnace to become char, the percentage of moisture and volatile matter of CC significantly reduced to 5.271 % and 42.958%, respectively. Subsequently, the microwave-assisted activation process gives a significant change to CCAC in terms of its moisture, volatile matter, and fixed carbon [42, 43]. According to Luqman et al. [44], thermal decomposition induced by intense heating enhances fixed carbon formation and substantially lowers volatile matter content. Furthermore, the ash content of CCAC (9.699%) is within an acceptable range, considering that ash is non-porous and does not participate in the adsorption mechanism. These results are supported by the findings of Aziz et al. [39], who reported an ash content of 8.19% for Nephelium lappaceum L. peel–derived AC prepared using the same method. The elemental analysis agrees with the proximate analysis, where CCAC shows a dominant carbon (C) content of 65.04% compared to hydrogen (H), sulphur (S), nitrogen (N), and other elements. Based on these data, Sun et al. [45] concluded that the samples are carbon-rich chars.

Table 6. Proximate and elemental analysis of samples

Samples	Proximate analysis (%)				Elemental analysis (%)			
	Moisture	Volatile matter	Fixed carbon	Ash	C	H	S	(N+Others)
CC	6.468	72.234	18.212	3.09	47.14	3.82	0.21	48.83
Char	5.271	42.958	41.956	9.815	64.85	3.91	0.46	30.78
CCAC	3.568	27.786	58.947	9.699	65.04	4.20	0.37	30.39

Figures 5-a and 5-b presents the FTIR spectra of CC, char, and CCAC and the proposed interaction mechanism between CP molecules and the functional groups of CCAC, respectively. CC exhibits distinct functional groups characteristic of cellulose, hemicellulose, and lignin, including a sharp carbonyl stretching band at 1743 cm^{-1}, a strong C–O stretching peak at 1234 cm^{-1}, and alkene =C–H bending around 1000 cm^{-1}. Upon carbonization (green line), the intensity of oxygenated functional groups decreased, while new peaks appeared, notably the carbonyl C=O stretching at ~1699 cm^{-1} and N–O symmetric stretching near 1550 cm^{-1}, indicating partial degradation of biopolymers and the formation of aromatic and nitrogen-containing structures. After microwave-assisted activation (blue line), many of the original lignocellulosic functional groups were eliminated, confirming extensive decomposition of cellulose and lignin**.** Nevertheless, CCAC retained several key functional group such as CH_2 stretching at 2920 cm^{-1}, carbonyl C=O stretching (1666–1685 cm^{-1}), aromatic C=C stretching with overlapping N–H bending (1585–1600 cm^{-1}), C–O stretching and cyclic vibrations (1050–1260 cm^{-1}), and aromatic =C–H out-of-plane bending at 750–920 cm^{-1} which are required for adsorption.

As illustrated in Figure 5-b, the adsorption of CP onto CCAC is governed by multiple non-covalent interactions. Among these, π–π stacking between the aromatic ring of CP and the graphitic C=C domains of CCAC, which is proposed as the dominant mechanism due to the high aromaticity of the AC surface. Hydrogen bonding also contributes significantly through interactions between the hydroxyl (–OH) and amide (–NH) groups of CP and the oxygen-containing functional groups (C=O and C–O) on CCAC, as supported by FTIR analysis. Dipole–dipole interactions between the polar groups of CP ($–NO_2$, –C=O, and $–CHCl_2$) and residual polar sites on the carbon surface further enhance adsorption. In addition to these surface interactions, pore filling within the developed microporous structure of CCAC plays an important role in accommodating CP molecules. Weak van der Waals forces provide secondary stabilization. Overall, π–π interactions and pore filling are considered the primary

mechanisms, while hydrogen bonding and dipole interactions act synergistically. A similar mechanism was proposed by Mohamad Yusop et al. [46] for the adsorption of CP using rattan waste, involving various interactions, including hydrogen bonding, π–π interactions, dipole–dipole interactions, and ion–dipole interactions. The presence of ion–dipole interactions was attributed to the copper metal used as a medium to functionalize the carbon surface, which also contributed to the interaction with CP molecules.

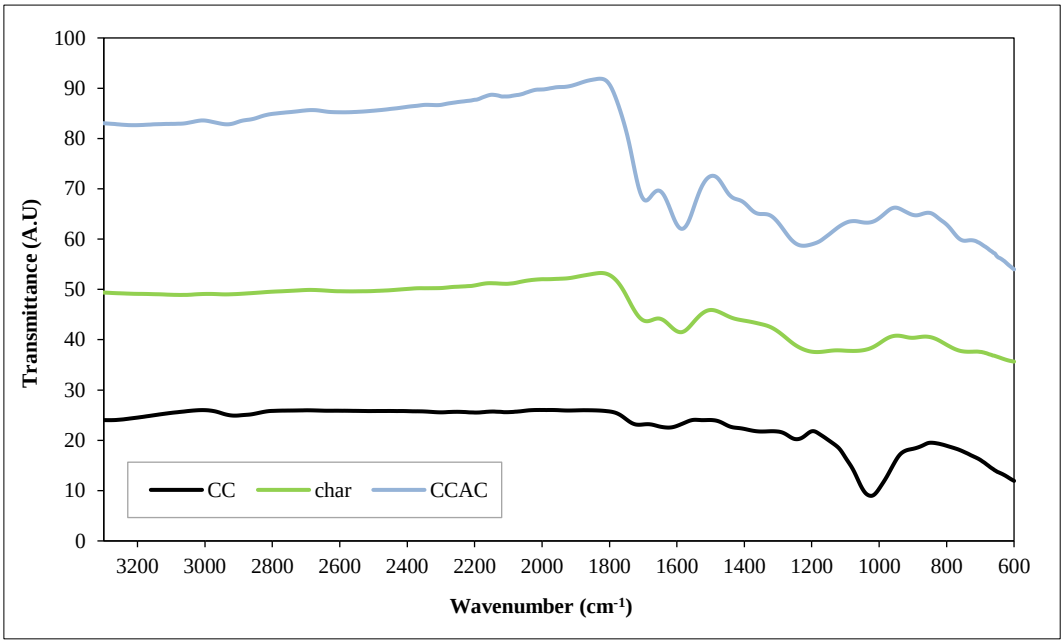

(a)

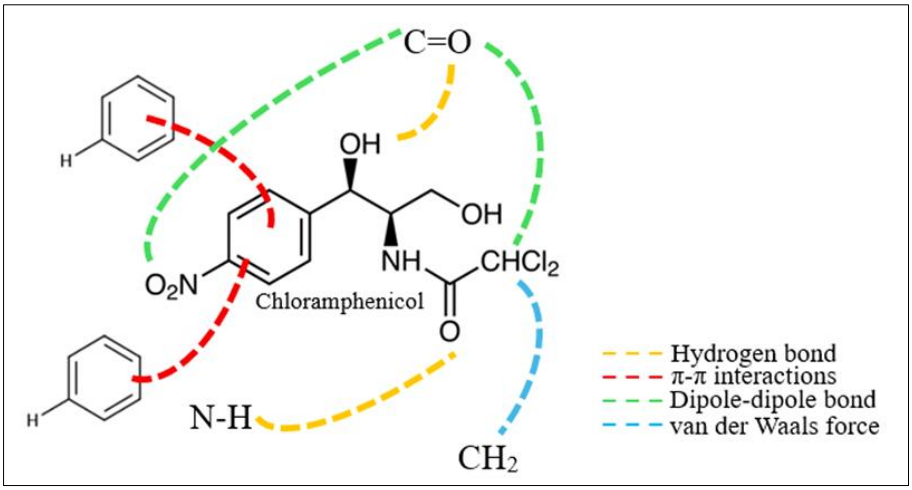

(b)

Figure 5. (a) Surface chemistry of the samples and (b) possible mechanism between the CP molecule and the CCAC functional groups

3-6- Removal of CP

The removal of CP was systematically evaluated by the adsorption capacity of CCAC under different conditions, including contact time and initial concentration, percentage removal, solution temperature, and solution pH in Figures 6- and 6-d). As depicted in Figure 6-a and 6-b, the adsorption capacity of CCAC increased from 4.85 to 20.68 mg/g with the rise in CP concentration from 5 to 30 mg/L, achieving up to 99% removal efficiency. This increase reflects the stronger driving force for mass transfer at higher concentrations, which promotes CP uptake at the available active sites [40, 47]. However, the removal efficiency decreased at higher concentrations, which is attributable to the saturation of adsorption sites because at lower CP concentrations, most of the adsorption sites remain unoccupied, allowing CP molecules to easily access and bind [48]. Mohamad Yusop et al. [46] reported the trend in the adsorption of CP using copper metal–functionalized carbon derived from rattan waste. This behavior was attributed to higher CP concentrations, which increased the ratio of CP molecules relative to the available active sites, thereby reducing removal efficiency.

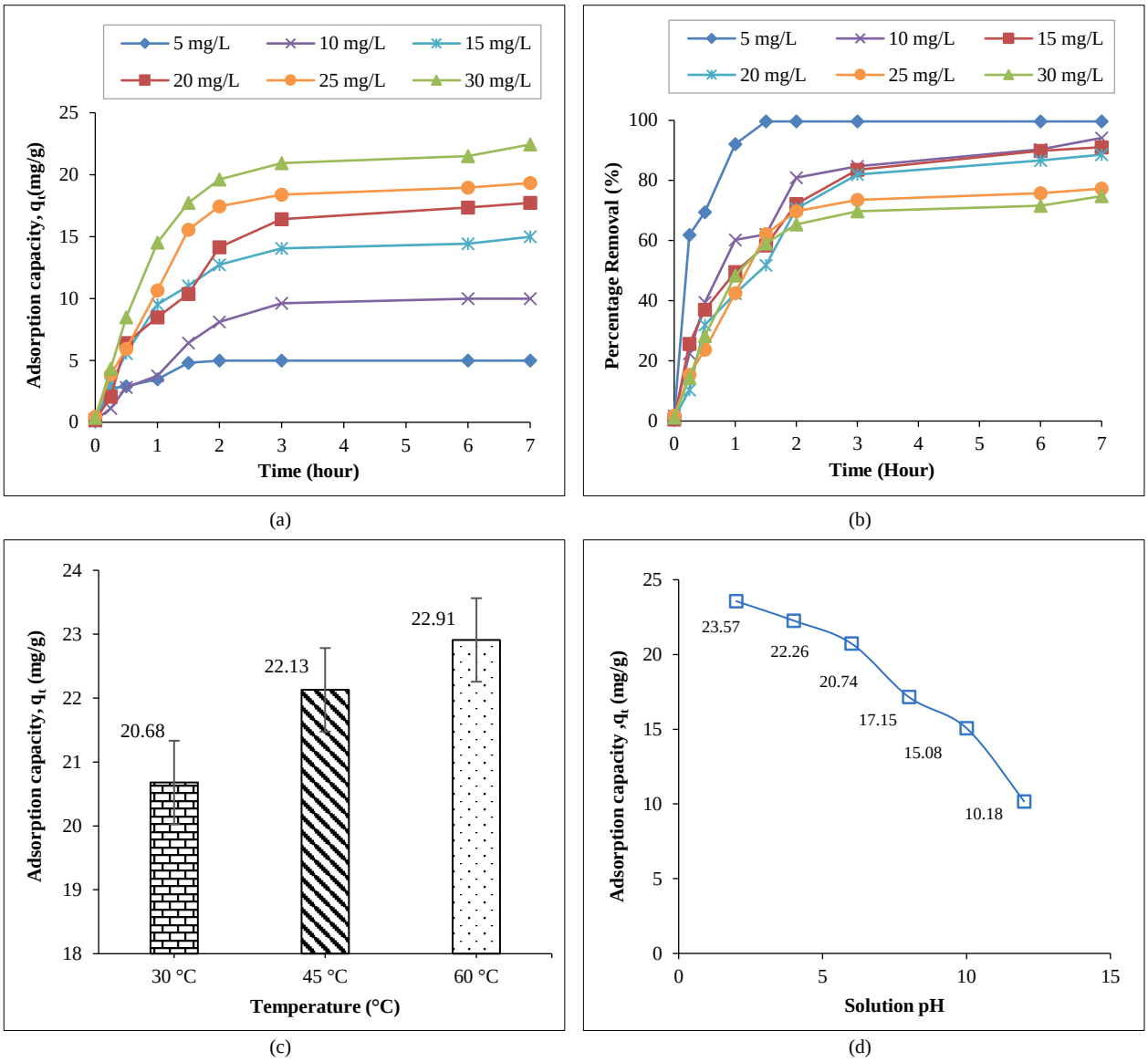

Figure 6. Adsorption studies of (a) Contact time and initial concentrations, (b) CP removal, (c) solution temperatures, and (d) solution pH

The result of the effect of varied temperature (30, 45, and 60 °C) is presented in Figure 6-c. It was observed that with an increase in temperature, the adsorption capacity increased from 20.68 to 22.91 mg/g, showing an endothermic process [3]. The enhanced adsorption at elevated temperatures can be attributed to increased molecular mobility and diffusion of CP molecules from the bulk solution toward CCAC pores and surface sites [49]. In addition, higher temperatures caused a reduction in solution viscosity, which tends to facilitate faster intraparticle diffusion, hence allowing more CP molecules to interact with the available active sites.

The adsorption of CP was further examined across a pH range of 2.0 –12.0. The highest adsorption capacity of 23.57 mg/g was obtained at pH 2, while the lowest value of 10.18 mg/g was obtained at pH 12, as shown in Figure 6-d). The strong pH dependence of CP adsorption can be explained by considering both CP speciation and the surface charge behavior of CCAC. CP has a reported pKa value of approximately 5.5–5.7, associated with the dissociation of its phenolic hydroxyl group [50]. At pH values below its pKa, CP predominantly exists in a neutral molecular form, whereas at pH values above its pKa, it increasingly converts to its negatively charged phenolate form. Under strongly acidic conditions (pH 2), CP remains largely neutral, while the surface functional groups of CCAC are protonated, minimising electrostatic repulsion and promoting adsorption through π–π interactions, hydrogen bonding, and pore filling. In contrast, at neutral to alkaline pH (7–12), both the deprotonated CP molecules and negatively charged CCAC surface lead to electrostatic repulsion, along with competition from hydroxide ions, thereby reducing adsorption efficiency [29]. Other studies have also reported that CP adsorption is favoured under acidic conditions [51]. For example, Anthonysamy et al. [52] reported that CP removal using coconut husk–derived activated carbon decreased with increasing solution pH due to the molecular structure of CP, which contains nitro, hydroxyl, and amide groups. These functional groups dissociate at different pH levels, causing CP to exhibit various ionic charge properties.

3-7- MT Model and Simulation

Figure 7 presents the MT model, where the symbols with and without lines represent the predicted and experimental CP concentrations, respectively. From Table 7, the MT model generated relatively high R^2 values at a minimum of 0.90 from 5 to 30 mg/L of CP, indicating the model fitted accurately between predicted and experimental data. Besides, the calculated ($Q_{e,cal}$) and experimental ($Q_{e,exp}$) adsorption capacity at the equilibrium stage produced a relatively low error in the range of 1 to 5%, showing a good agreement that the developed model was suitable for fitting to the kinetic data. It is important to highlight that the MT model provides insight into the rate coefficients governing CP transport from the bulk solution to the solid phase of CCAC ((k_m) as well as the adsorption rate during intraparticle pore diffusion ((k_{mT}). As presented in Table 7, k_m ranged from 3.54 to 6.46 $x\ 10^{-3}$ mg.m. L^{-1} s^{-1}, while k_{mT} ranged between 3.35 to 3.57 s^{-1}. The observed reduction in $k_m$value can be attributed to the gradual increase in mass transfer resistance as adsorption progresses. As the active sites on the CCAC surface become progressively occupied, the interaction between CP molecules and the adsorbent surface slows down, thereby decreasing the overall mass transfer rate [53]. Furthermore, at higher initial CP concentrations, stronger mass transfer resistance and intensified competition among CP molecules for available active sites further reduce the mass transfer rate. In addition, Yusop et al. [54] reported lower k_m values under the Polymath mass transfer (PMT) model, attributing the decrease to a slower adsorption process caused by increasing diffusion resistance. Notably, the MT model accurately predicted the adsorption surface area (a_{mT}) of CCAC as 650.45 m^2/g, which closely aligns with the experimentally determined external surface area (mesopore-associated) of 623.45 m^2/g. A similar approach was employed by Rosli et al. [55] to predict the surface area of a pineapple peel–based adsorbent, reporting an error percentage of only 0.3145%. This demonstrates the distinct advantage of the MT model, particularly its capability to predict the effective surface area actively involved in the adsorption process.

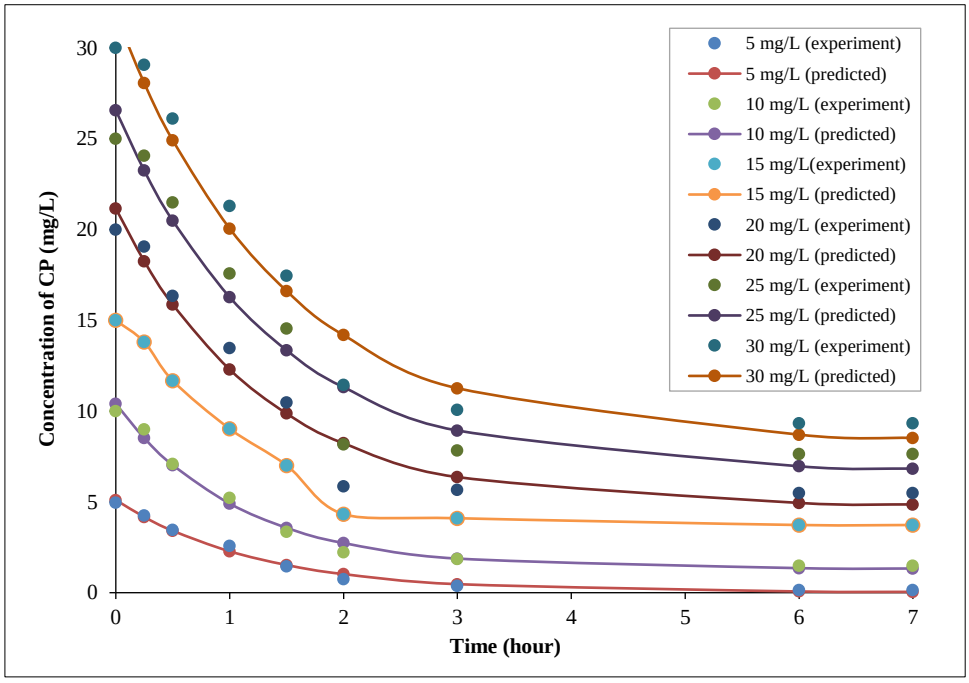

Figure 7. Concentration of CP versus time for predicted and experimental data

Table 7. MT parameters for the removal of CP

Initial concentration (mg/L)	Mass transfer model						
	$Q_{e,exp}$ (mg/g)	$Q_{e,cal}$ (mg/g)	$k_{m\ x\ 10^{-3}}$ (mg.m. L^{-1} s^{-1})	k_{MT} (s^{-1})	a_{mT} (m^2/g)	R^2	Error (%)
5	4.85	4.95	6.46	3.35	645.58	0.99	2.06
10	8.51	8.67	5.53	3.33	652.95	0.99	1.88
15	11.27	11.60	5.51	3.38	651.00	0.98	2.93
20	14.52	15.14	4.50	3.45	650.61	0.96	4.27
25	17.35	18.17	3.49	3.48	649.06	0.95	4.73
30	20.68	21.48	3.54	3.57	653.50	0.97	3.87
Average					**650.45**	**0.97**	**3.29**

4- Conclusion

This study successfully developed a corn cob–derived activated carbon (CCAC) for chloramphenicol (CP) removal and integrated the response surface methodology (RSM) optimization with mass transfer (MT) modeling. The optimal preparation conditions (3.86 min activation time, 616 W radiation power, and 2.5 g/g impregnation ratio (IR)) produced CCAC with a high BET surface area (832.68 m^2/g), well-developed mesoporosity, and a maximum adsorption capacity of 20.68 mg/g at 30°C. Statistical validation confirmed the adequacy of the quadratic RSM model ($R^2>0.90$), demonstrating that radiation power and IR were dominant factors influencing CP removal, while the activation time significantly affected yield. Structural characterization and proximate analysis revealed that microwave-assisted physicochemical activation enhanced fixed carbon content, reduced volatile matter, and generated a highly porous structure favorable for CP removal.

An adsorption capacity of 20.68 mg/g was obtained at an initial CP concentration of 30 mg/L at 30°C, which increased to 22.91 mg/g at 60°C, indicating the endothermic nature of the process. The highest adsorption capacity (23.57 mg/g) was achieved at pH 2, further suggesting the role of electrostatic interactions and functional group dissociation in the adsorption behavior of CP on the CCAC. The developed MT model accurately predicted equilibrium adsorption capacity with a low average error (3.29%) and $R^2 \geq 0.90$. The observed decrease in mass transfer coefficient (from 6.46×10^{-3} to 3.54×10^{-3} $mg\cdot m\cdot L^{-1}\cdot s^{-1}$) at higher concentrations indicates increasing diffusion resistance and progressive site saturation. Overall, this integrated optimization–modeling framework provides both mechanistic insight and predictive capability, highlighting CCAC as a sustainable and promising adsorbent for antibiotic-contaminated water treatment.

5- Declarations

5-1- Author Contributions

Conceptualization, M.R.M.R., M.A.A., and N.F.S.; methodology, M.R.M.R.; software, N.F.S.; validation, A.W.M., M.S.T., and E.I.O.; formal analysis, M.R.M.R.; investigation, M.R.M.R.; resources, A.W.M. and M.A.A.; data curation, M.R.M.R.; writing—original draft preparation, M.R.M.R.; writing—review and editing, E.I.O.; visualization, N.F.S.; supervision, M.A.A., N.F.S., and A.W.M.; project administration, M.S.T.; funding acquisition, A.W.M. and M.A.A. All authors have read and agreed to the published version of the manuscript.

5-2- Data Availability Statement

The data presented in this study are available on request from the corresponding author.

5-3- Funding

This research was supported by the Malaysian Ministry of Higher Education under the Fundamental Research Grant Scheme (project code: FRGS/1/2023/TK05/USM/02/8) and Integrated Water Processing Technologies Research Group, University of Sharjah (project cost code is: 331826).

5-4- Institutional Review Board Statement

Not applicable.

5-5- Informed Consent Statement

Not applicable.

5-6- Conflicts of Interest

The authors declare that there is no conflict of interest regarding the publication of this manuscript. In addition, the ethical issues, including plagiarism, informed consent, misconduct, data fabrication and/or falsification, double publication and/or submission, and redundancies have been completely observed by the authors.

6- References

[1] Singh, A., Pratap, S. G., & Raj, A. (2024). Occurrence and dissemination of antibiotics and antibiotic resistance in aquatic environment and its ecological implications: a review. Environmental Science and Pollution Research, 31(35), 47505–47529. doi:10.1007/s11356-024-34355-x.

[2] Okeke, E. S., Chukwudozie, K. I., Nyaruaba, R., Ita, R. E., Oladipo, A., Ejeromedoghene, O., Atakpa, E. O., Agu, C. V., & Okoye, C. O. (2022). Antibiotic resistance in aquaculture and aquatic organisms: a review of current nanotechnology applications for sustainable management. Environmental Science and Pollution Research, 29(46), 69241–69274. doi:10.1007/s11356-022-22319-y.

[3] Li, H., Zhu, H., Qiu, J., Zheng, D., Gao, L., Zhou, D., & Xu, D. (2024). Adsorption behavior of chloramphenicol on an activated carbon from pomelo peel using KHCO3 activator. New Journal of Chemistry, 48(16), 7081–7091. doi:10.1039/d3nj05838g.

[4] Nabilah Mohd Noor, N., Hazirah Kamaruzaman, N., Al-Gheethi, A., Maya Saphira Radin Mohamed, R., & Hossain, M. S. (2023). Degradation of antibiotics in aquaculture wastewater by bio-nanoparticles: A critical review. Ain Shams Engineering Journal, 14(7), 101981. doi:10.1016/j.asej.2022.101981.

[5] Skoupá, K., Šťastný, K., & Sládek, Z. (2022). Anabolic Steroids in Fattening Food-Producing Animals—A Review. Animals, 12(16), 2115. doi:10.3390/ani12162115.

[6] Ghazal, H., Koumaki, E., Hoslett, J., Malamis, S., Katsou, E., Barcelo, D., & Jouhara, H. (2022). Insights into current physical, chemical and hybrid technologies used for the treatment of wastewater contaminated with pharmaceuticals. Journal of Cleaner Production, 361, 132079. doi:10.1016/j.jclepro.2022.132079.

[7] Nguyen, L. M., Nguyen, N. T. T., Nguyen, T. T. T., Nguyen, T. T., Nguyen, D. T. C., & Tran, T. Van. (2022). Occurrence, toxicity and adsorptive removal of the chloramphenicol antibiotic in water: a review. Environmental Chemistry Letters, 20(3), 1929–1963. doi:10.1007/s10311-022-01416-x.

[8] Harun, M. H. Z. M., & Ahmad, A. L. (2023). Removal of low concentration ibuprofen using green diluent and novel formulated supported ionic liquid membrane. Journal of Environmental Chemical Engineering, 11(3), 109972. doi:10.1016/j.jece.2023.109972.

[9] Mohd Ramli, M. R., Mat Radzi, N. H., Mohamad Esham, M. I., Alsebaeai, M. K., & Ahmad, A. L. (2021). Advanced Application and Fouling Control in Hollow Fibre Direct Contact Membrane Distillation (HF-DCMD). Arabian Journal for Science and Engineering, 46(7), 6439–6456. doi:10.1007/s13369-020-05006-3.

[10] Anjali, R., & Shanthakumar, S. (2019). Insights on the current status of occurrence and removal of antibiotics in wastewater by advanced oxidation processes. Journal of Environmental Management, 246, 51–62. doi:10.1016/j.jenvman.2019.05.090.

[11] Zulfiqar, N., Nadeem, R., & Musaimi, O. A. (2024). Photocatalytic degradation of antibiotics via exploitation of a magnetic nanocomposite: a green nanotechnology approach toward drug-contaminated wastewater reclamation. ACS omega, 9(7), 7986-8004. doi:10.1021/acsomega.3c08116.

[12] Algaradah, M. M. (2024). MXene-based adsorbent materials for pollutants removal from water: Current challenges and future prospects. Inorganic Chemistry Communications, 161, 112113. doi:10.1016/j.inoche.2024.112113.

[13] Ramli, M. R. M., Shoparwe, N. F., & Ahmad, M. A. (2024). Adsorption of Acetaminophen onto activated carbon derived from corn cobs: Optimizations by using response surface methodology. Journal of Physics: Conference Series, 2907(1), 12012. doi:10.1088/1742-6596/2907/1/012012.

[14] Paulino, R., Tamburic, B., Stuetz, R. M., Zamyadi, A., Crosbie, N., & Henderson, R. K. (2023). Critical review of adsorption and biodegradation mechanisms for removal of biogenic taste and Oduor compounds in granular and biological activated carbon contactors. Journal of Water Process Engineering, 52, 103518. doi:10.1016/j.jwpe.2023.103518.

[15] Jagadeesh, N., & Sundaram, B. (2023). Adsorption of Pollutants from Wastewater by Biochar: A Review. Journal of Hazardous Materials Advances, 9, 100226. doi:10.1016/j.hazadv.2022.100226.

[16] Afolabi, I. C., Popoola, S. I., & Bello, O. S. (2020). Modeling pseudo-second-order kinetics of orange peel-paracetamol adsorption process using artificial neural network. Chemometrics and Intelligent Laboratory Systems, 203, 104053. doi:10.1016/j.chemolab.2020.104053.

[17] Mohamad Yusop, M. F., Nasehir Khan, M. N., Zakaria, R., Abdullah, A. Z., & Ahmad, M. A. (2023). Mass transfer simulation on Remazol brilliant blue R dye adsorption by optimized teak wood Based activated carbon. Arabian Journal of Chemistry, 16(6), 104780. doi:10.1016/j.arabjc.2023.104780.

[18] Cunha, M. R., Lima, E. C., Lima, D. R., da Silva, R. S., Thue, P. S., Seliem, M. K., Sher, F., dos Reis, G. S., & Larsson, S. H. (2020). Removal of captopril pharmaceutical from synthetic pharmaceutical-industry wastewaters: Use of activated carbon derived from Butia catarinensis. Journal of Environmental Chemical Engineering, 8(6), 104506. doi:10.1016/j.jece.2020.104506.

[19] Song, T., Zhang, Y., Wei, H., Wang, Y., & Gao, Y. (2025). Iron-modified biochar from fermented grain residues for enhanced oxytetracycline degradation via periodate activation. Ain Shams Engineering Journal, 16(12), 103789. doi:10.1016/j.asej.2025.103789.

[20] Gatrouni, M., Asses, N., Bedia, J., Belver, C., Molina, C. B., & Mzoughi, N. (2024). Acetaminophen adsorption on carbon materials from Citrus waste. C, 10(2), 53. doi:10.3390/c10020053.

[21] Mohd Ramli, M. R., Shoparwe, N. F., & Ahmad, M. A. (2023). Methylene Blue Removal Using Activated Carbon Adsorbent from Jengkol Peel: Kinetic and Mass Transfer Studies. Arabian Journal for Science and Engineering, 48(7), 8585–8594. doi:10.1007/s13369-022-07141-5.

[22] Khan, M. N. N., Yusop, M. F. M., Latiff, M. F. P. M., & Ahmad, M. A. (2023). Utilization of landscape biomass waste as activated carbon to scavenge oxytetracycline: Attraction mechanism, batch and continuous studies. Arabian Journal of Chemistry, 16(11), 105256. doi:10.1016/j.arabjc.2023.105256.

[23] Mensah, K., Samy, M., Mahmoud, H., Fujii, M., & Shokry, H. (2023). Rapid adsorption of sulfamethazine on mesoporous graphene produced from plastic waste: optimization, mechanism, isotherms, kinetics, and thermodynamics. International Journal of Environmental Science and Technology, 20(9), 9717–9732. doi:10.1007/s13762-022-04646-2.

[24] Ratnawati, R., Wulandari, R., Kumoro, A. C., & Hadiyanto, H. (2022). Response Surface Methodology for Formulating PVA/Starch/Lignin Biodegradable Plastic. Emerging Science Journal, 6(2), 238–255. doi:10.28991/esj-2022-06-02-03.

[25] Almahbashi, N. M. Y., Kutty, S. R. M., Ayoub, M., Noor, A., Salihi, I. U., Al-Nini, A., Jagaba, A. H., Aldhawi, B. N. S., & Ghaleb, A. A. S. (2021). Optimization of Preparation Conditions of Sewage sludge based Activated Carbon. Ain Shams Engineering Journal, 12(2), 1175–1182. doi:10.1016/j.asej.2020.07.026.

[26] Qian Sun, Kamaruddin, M. A. B., Kai Huang, Yun Cao, Mohd Suffian Yusoff, & Yong Cheng. (2025). Study on Preparation of Nano Humic Acid and Adsorption Effect of Heavy Metals in Soil. Emerging Science Journal, 9(5), 2350–2366. doi:10.28991/ESJ-2025-09-05-04.

[27] Shamsudin, M. S., Sellaoui, L., Ismail, S., Mohd Din, A. T., Khajavian, M., Bonilla-Petriciolet, A., & Badawi, M. (2025). Mechanistic insights of diclofenac adsorption on functionalized Clay-Based adsorptive Film: Bridging experimental and molecular dynamics findings. Separation and Purification Technology, 377, 134119. doi:10.1016/j.seppur.2025.134119.

[28] Yusop, M. F. M., Baharudin, M. H., Rashid, M. M., Alam, M. M., & Ahmad, M. A. (2025). Amoxicillin adsorption onto oil palm trunk- derived activated carbon: synthesis optimization, modelling of mass transfer and ultrasonic regeneration. Journal of Chemical Technology & Biotechnology, 100(6), 1310–1327. doi:10.1002/jctb.7864.

[29] Mohamad Yusop, M. F., Rashid, M. M., Alam, M. M., & Ahmad, M. A. (2025). Enhanced Cd2+ removal via deprotonated-mango trunk functionalized carbon: Optimization and F-test for linear and non-linear isotherm and kinetic models. Chemical Engineering Research and Design, 220, 96–116. doi:10.1016/j.cherd.2025.07.004.

[30] Abd Khalil, A. T., Mohamad Yusop, M. F., & Ahmad, M. A. (2026). Remediation of oxytetracycline-contaminated aqueous solution utilizing functionalized coffee ground waste-derived activated carbon. Particuology, 111, 11–26. doi:10.1016/j.partic.2026.01.027.

[31] Mohamad Yusop, M. F., Tamar Jaya, M. A., Idris, I., Abdullah, A. Z., & Ahmad, M. A. (2023). Optimization and mass transfer simulation of Remazol brilliant blue R dye adsorption onto meranti wood based activated carbon. Arabian Journal of Chemistry, 16(5), 104683. doi:10.1016/j.arabjc.2023.104683.

[32] Rashidi, N. A., & Yusup, S. (2017). A review on recent technological advancement in the activated carbon production from oil palm wastes. Chemical Engineering Journal, 314, 277–290. doi:10.1016/j.cej.2016.11.059.

[33] Aziz, A., Hassan, H., & Ahmad, M. A. (2023). Chloramphenicol and methylene blue adsorption by modestly treated paper sewage sludge-based activated carbon. Chemical Papers, 77(12), 7551–7561. doi:10.1007/s11696-023-03052-3.

[34] Nasran Nasehir Khan, M., Firdaus Mohamad Yusop, M., Faizal Pakir Mohamed Latiff, M., & Azmier Ahmad, M. (2023). Alteration of Tecoma chip wood waste into microwave-irradiated activated carbon for amoxicillin removal: Optimization and batch studies. Arabian Journal of Chemistry, 16(10), 105110. doi:10.1016/j.arabjc.2023.105110.

[35] Abdillah, N., Mohamad Yusop, M. F., Mokhtar Kamal, N. H., & Azmier Ahmad, M. (2023). Single-stage microwave-irradiated activated carbon from corncob for ammonia nitrogen removal: Batch, attraction mechanism and regeneration studies. Inorganic Chemistry Communications, 158, 111672. doi:10.1016/j.inoche.2023.111672.

[36] Mohd Zainorin, N. A., Zakaria, R., Abdul Malik, M. F. I., & Ahmad, M. A. (2025). Physicochemical activation of activated carbon derived from mangrove wood via microwave heating technique: Optimization and batch studies. IOP Conference Series: Earth and Environmental Science, 1516(1), 12022. doi:10.1088/1755-1315/1516/1/012022.

[37] Ramli, M. R. M., Shoparwe, N. F., Ahmad, M. A., & Yusop, M. F. M. (2024). Acetaminophen removal using porous activated carbon derived from corn cob: optimization and mass transfer modelling. Journal of Chemical Technology & Biotechnology, 99(9), 2088–2106. doi:10.1002/jctb.7712.

[38] Kuptajit, P., Sano, N., Nakagawa, K., & Suzuki, T. (2021). A study on pore formation of high surface area activated carbon prepared by microwave-induced plasma with KOH (MiWP-KOH) activation: Effect of temperature-elevation rate. Chemical Engineering and Processing - Process Intensification, 167, 108511. doi:10.1016/j.cep.2021.108511.

[39] Aziz, A., Mohamad Yusop, M. F., & Ahmad, M. A. (2024). Harnessing microwave energy to transform Nephelium lappaceum L. peel into activated carbon for chloramphenicol eradication in aqueous solutions. Materials Chemistry and Physics, 318, 129311. doi:10.1016/j.matchemphys.2024.129311.

[40] Nasehir Khan, M. N., Mohd Arif Zainol, M. R. R., Mohamad Yusop, M. F., & Ahmad, M. A. (2025). Turning waste into wonder: Arsenic removal using rice husk based activated carbon. Journal of Engineering Research, 13(3), 2503–2516. doi:10.1016/j.jer.2024.09.010.

[41] Zhang, P., Duan, W., Peng, H., Pan, B., & Xing, B. (2022). Functional Biochar and Its Balanced Design. ACS Environmental Au, 2(2), 115–127. doi:10.1021/acsenvironau.1c00032.

[42] Mohamad Yusop, M. F., Mohd Johan Jaya, E., & Ahmad, M. A. (2022). Single-stage microwave assisted coconut shell based activated carbon for removal of Zn(II) ions from aqueous solution – Optimization and batch studies. Arabian Journal of Chemistry, 15(8), 104011. doi:10.1016/j.arabjc.2022.104011.

[43] Saheed, I. O., Zairuddin, N. I., Nizar, S. A., Hanafiah, M. A. K. M., Latip, A. F. A., & Suah, F. B. M. (2024). Adsorption potential of CuO-embedded chitosan bead for the removal of acid blue 25 dye. Ain Shams Engineering Journal, 15(12), 103125. doi:10.1016/j.asej.2024.103125.

[44] Luqman, F., Mohd Din, A. T., Md Nor, N., Johan Jaya, E. M., & Azmier Ahmad, M. (2025). Synthesizing palm kernel shell-based activated carbon for chloramphenicol removal via a single-step microwave heating. Journal of Physics: Conference Series, 3003(1), 12034. doi:10.1088/1742-6596/3003/1/012034.

[45] Sun, S., Yu, Q., Li, M., Zhao, H., & Wu, C. (2019). Preparation of coffee-shell activated carbon and its application for water vapor adsorption. Renewable Energy, 142, 11–19. doi:10.1016/j.renene.2019.04.097.

[46] Mohamad Yusop, M. F., Rashid, M. M., Alam, M. M., & Ahmad, M. A. (2025). Copper metal-functionalized carbon from rattan waste via microwave pyrolysis for enhanced chloramphenicol removal: Optimization and F-test study. Particuology, 100, 196–213. doi:10.1016/j.partic.2025.03.011.

[47] López-Bermúdez, N. L., Rodríguez-Torres, A. C., Otálvaro-Álvarez, Ángela M., & Peña-Guzmán, C. A. (2025). Phosphate Adsorption from Aqueous Solutions Using Eggshell and Sacha Inchi (Plukenetia volubilis) Mixture. Civil Engineering Journal, 11(7), 2918–2932. doi:10.28991/CEJ-2025-011-07-016.

[48] Gkika, D. A., Tolkou, A. K., Katsoyiannis, I. A., & Kyzas, G. Z. (2025). The adsorption-desorption-regeneration pathway to a circular economy: The role of waste-derived adsorbents on chromium removal. Separation and Purification Technology, 368, 132996. doi:10.1016/j.seppur.2025.132996.

[49] Sh. Gohr, M., Abd-Elhamid, A. I., El-Shanshory, A. A., & Soliman, H. M. A. (2022). Adsorption of cationic dyes onto chemically modified activated carbon: Kinetics and thermodynamic study. Journal of Molecular Liquids, 346, 118227. doi:10.1016/j.molliq.2021.118227.

[50] Sayler, B., Manship, A. J., Davis, J., Taylor, J., & Gilliam, L. (2025). Pharmacokinetics of Chloramphenicol and Chloramphenicol Glucuronide in Horses Following Administration Per Rectum or via Nasogastric Intubation. Journal of Veterinary Pharmacology and Therapeutics, 48(5), 397–404. doi:10.1111/jvp.13520.

[51] Lach, J. (2019). Adsorption of chloramphenicol on commercial and modified activated carbons. Water (Switzerland), 11(6), 1141. doi:10.3390/w11061141.

[52] Anthonysamy, S. I., Yusop, M. F. M., Ismail, H., & Ahmad, M. A. (2023). Chloramphenicol Removal from Aqueous Solution Using Sodium Bicarbonate-Impregnated Coconut Husk-Derived Activated Carbon: Optimization and Insight Mechanism Study. Arabian Journal for Science and Engineering, 48(12), 15999–16022. doi:10.1007/s13369-023-07933-3.

[53] Mohamad Yusop, M. F., Abdullah, A. Z., & Ahmad, M. A. (2024). Amoxicillin adsorption from aqueous solution by Cu(II) modified lemon peel based activated carbon: Mass transfer simulation, surface area prediction and F-test on isotherm and kinetic models. Powder Technology, 438, 119589. doi:10.1016/j.powtec.2024.119589.

[54] Yusop, M. F. M., Abdullah, A. Z., & Ahmad, M. A. (2023). Adsorption of Remazol brilliant blue R dye onto jackfruit peel based activated carbon: Optimization and simulation for mass transfer and surface area prediction. Inorganic Chemistry Communications, 158, 111721. doi:10.1016/j.inoche.2023.111721.

[55] Rosli, N. A., Ahmad, M. A., & Noh, T. U. (2025). Regeneration and mass transfer simulation for Remazol brilliant violet dye adsorption by pineapple peel–based adsorbent. Journal of Engineering Research, 13(2), 433–444. doi:10.1016/j.jer.2024.02.005.